Electronic Supplementary Information for

Pd@Rh Core-Shell Nanocrystals with Well-Defined Facets and Their Enhanced Catalytic Performance towards CO Oxidation

Sang-Il Choi,[ab] Allison Young,[c] Sujin R. Lee,[d] Cheng Ma,[e] Ming Luo,[a] Miaofang Chi,[e] Chia-Kuang Tsung*[c] and Younan Xia*[adf]

[a]The Wallace H. Coulter Department of Biomedical Engineering, Georgia Institute of Technology and Emory University, Atlanta, Georgia 30332, United States

[b]Department of Chemistry and Green-Nano Materials Research Center, Kyungpook National University, Daegu 41566, Republic of Korea.

[c]Department of Chemistry, Merkert Chemistry Center, Boston College, Chestnut Hill, Massachusetts 02467, United States

[d]School of Chemistry and Biochemistry, Georgia Institute of Technology, Atlanta, Georgia 30332, United States

[e]Materials Science and Technology Division, Oak Ridge National Laboratory, Oak Ridge, Tennessee 37830, United States

[f]School of Chemical and Biomolecular Engineering, Georgia Institute of Technology, Atlanta, Georgia 30332, United States

*Corresponding authors: frank.tsung@bc.edu (C.K.T. for CO oxidation measurements); younan.xia@bme.gatech.edu (Y.X. for synthesis and characterization)

Table S1. The average number (n) of Rh atomic layers calculated from the ICP−MS data for the Pd and Rh contents in the Pd@Rh core-shell nanocrystals, the weight percentage (wt%) of Rh obtained from the ICP−MS data, and the wt% of Rh derived from the average number of Rh atomic layers and the size of the Pd seeds such as octahedra and cubes.

Samples	Average number of Rh atomic layers (n)	wt% of Rh obtained from the ICP−MS data	wt% of Rh calculated from the value of n
Pd@Rh octahedra	2.1	42.2	39.8 (n=2)
Pd@Rh cubes	2.9	36.6	37.8 (n=3)

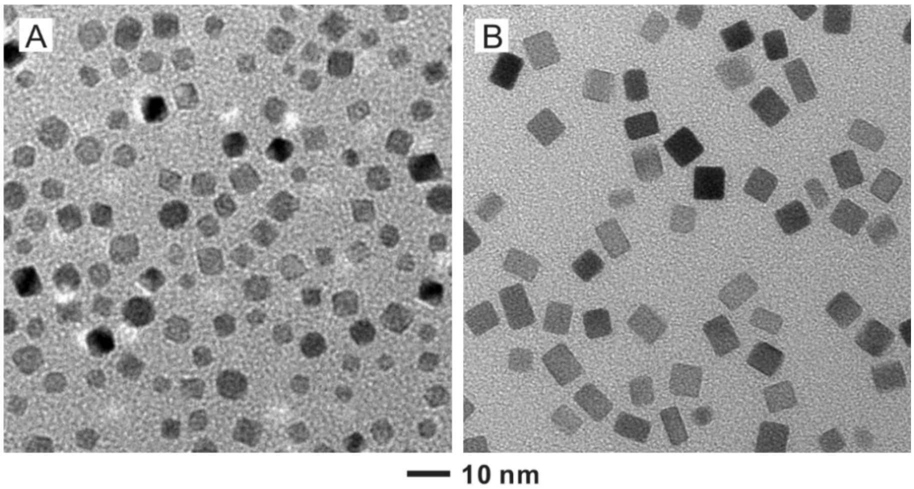

Fig. S1 TEM images of (A) Pd octahedra and (B) Pd cubes with average edge lengths of 6.4 and 7.2 nm, respectively, which served as seeds for the overgrowth of Rh.

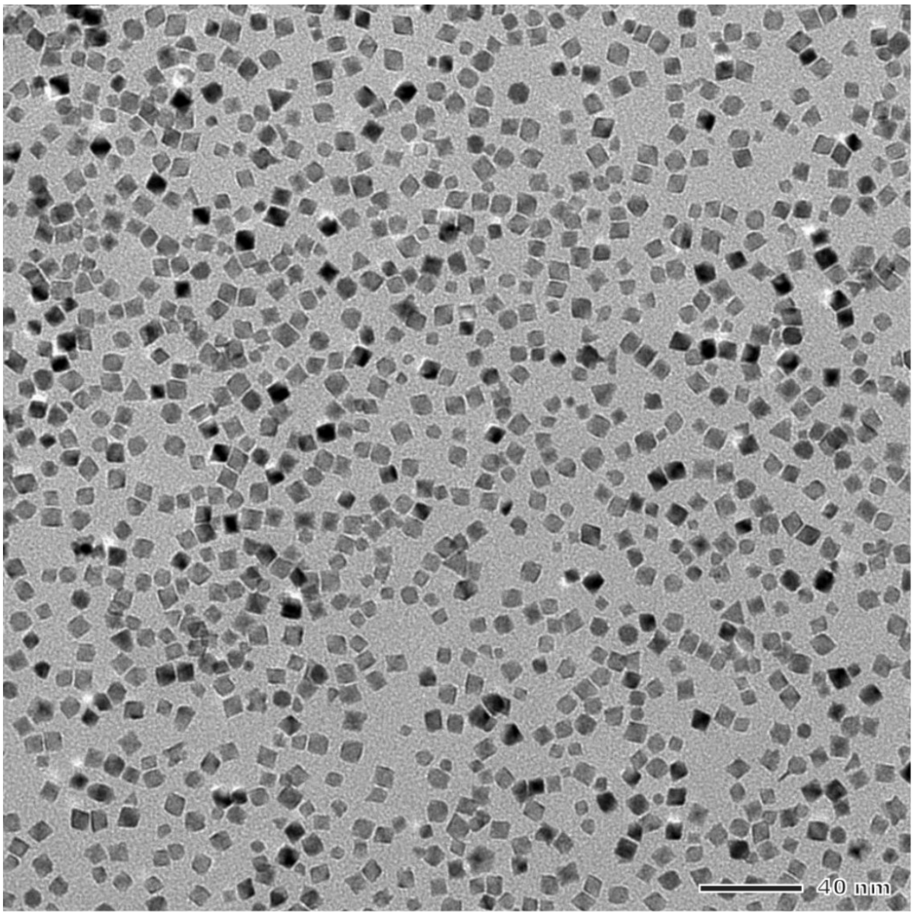

Fig. S2 TEM image of Pd@Rh core-shell octahedra at a relatively low magnification to show uniformity in both size and shape.

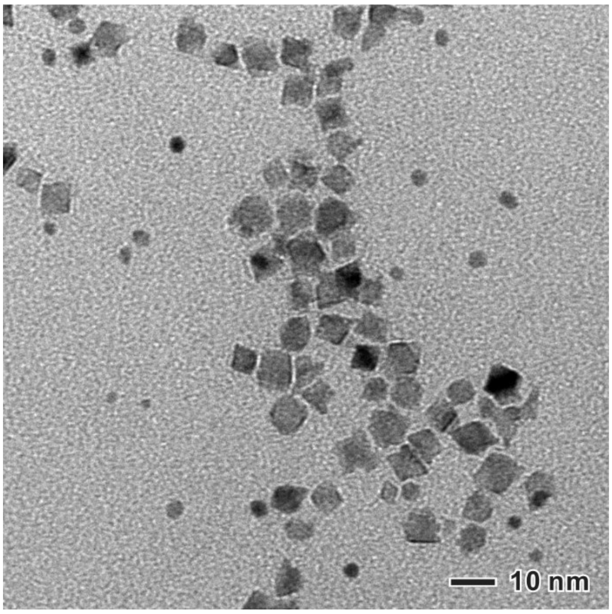

Fig. S3 TEM image of a product containing both Pd@Rh core-shell octahedra and small Rh nanocrystals when a larger volume (81 μL) of $Rh(OAc)_3$ solution was used while all other conditions were kept the same as the standard protocol.

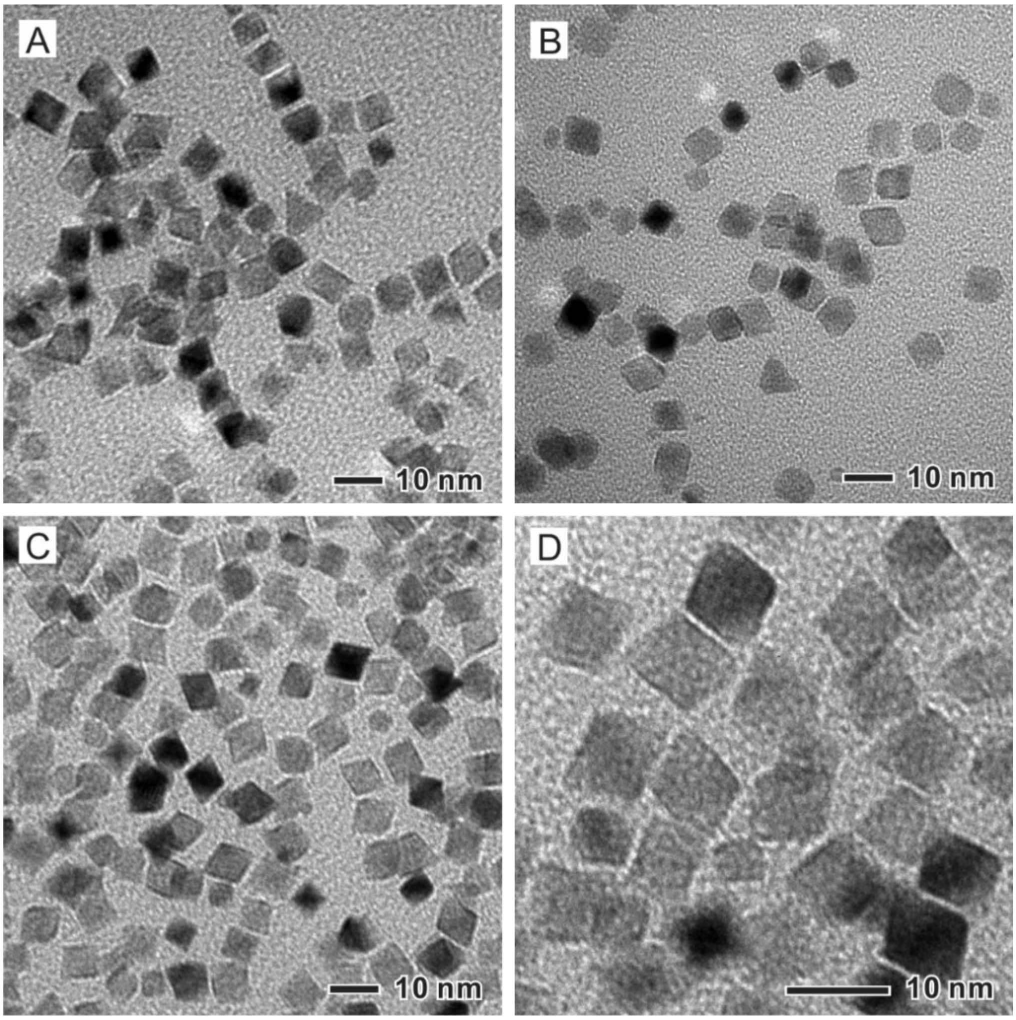

Fig. S4 TEM images of Pd@Rh core-shell octahedra prepared using different Rh precursors, including (A) $RhCl_3$, (B) $Rh(NO_3)_3$, and (C, D) $Rh(acac)_3$, respectively, using a protocol similar to what was used for the Pd@Rh octahedra shown in Fig. 1.

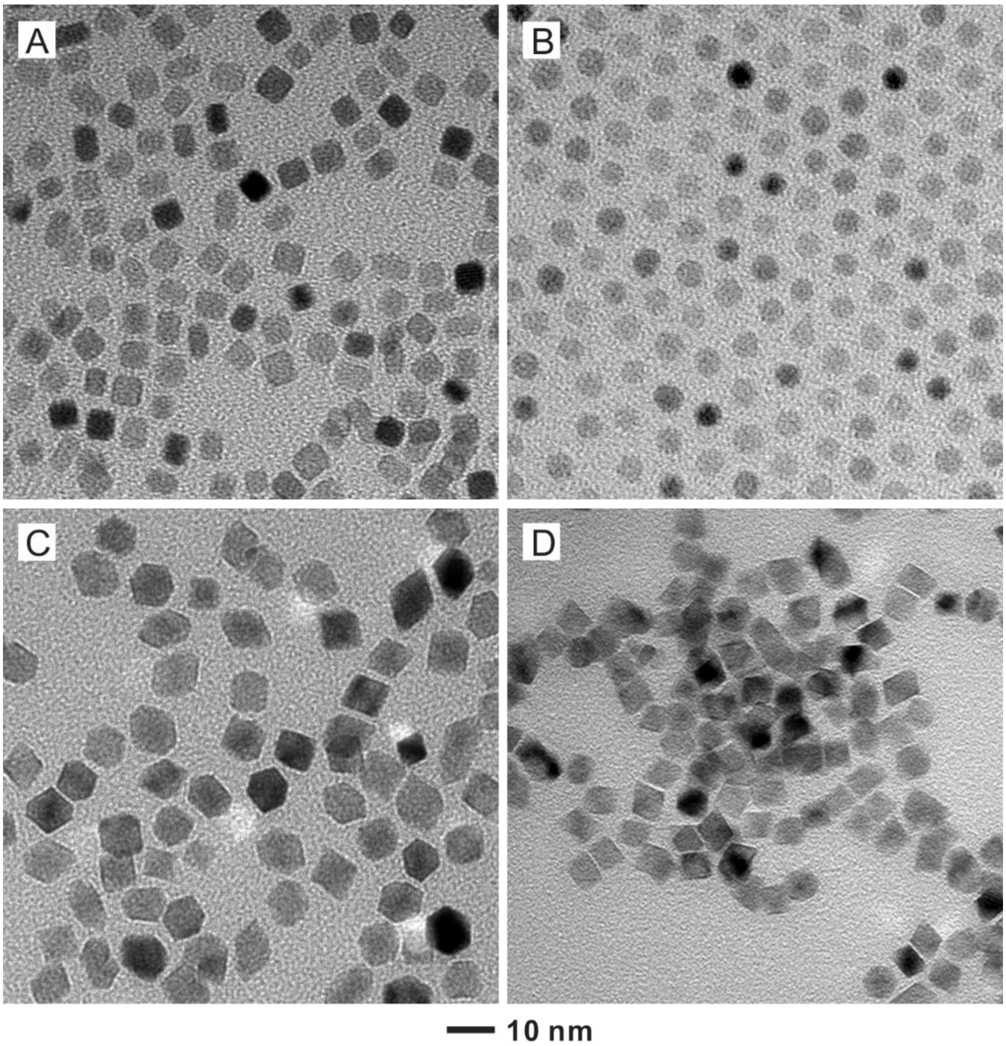

Fig. S5 TEM images of (A) Pd cubes and (B) Pd cuboctahedra. TEM images of Pd@Rh octahedra grown from the (C) cubic and (D) cuboctahedral, respectively, seeds of Pd, with a protocol similar to what was used for the Pd@Rh octahedra shown in Fig. 1.

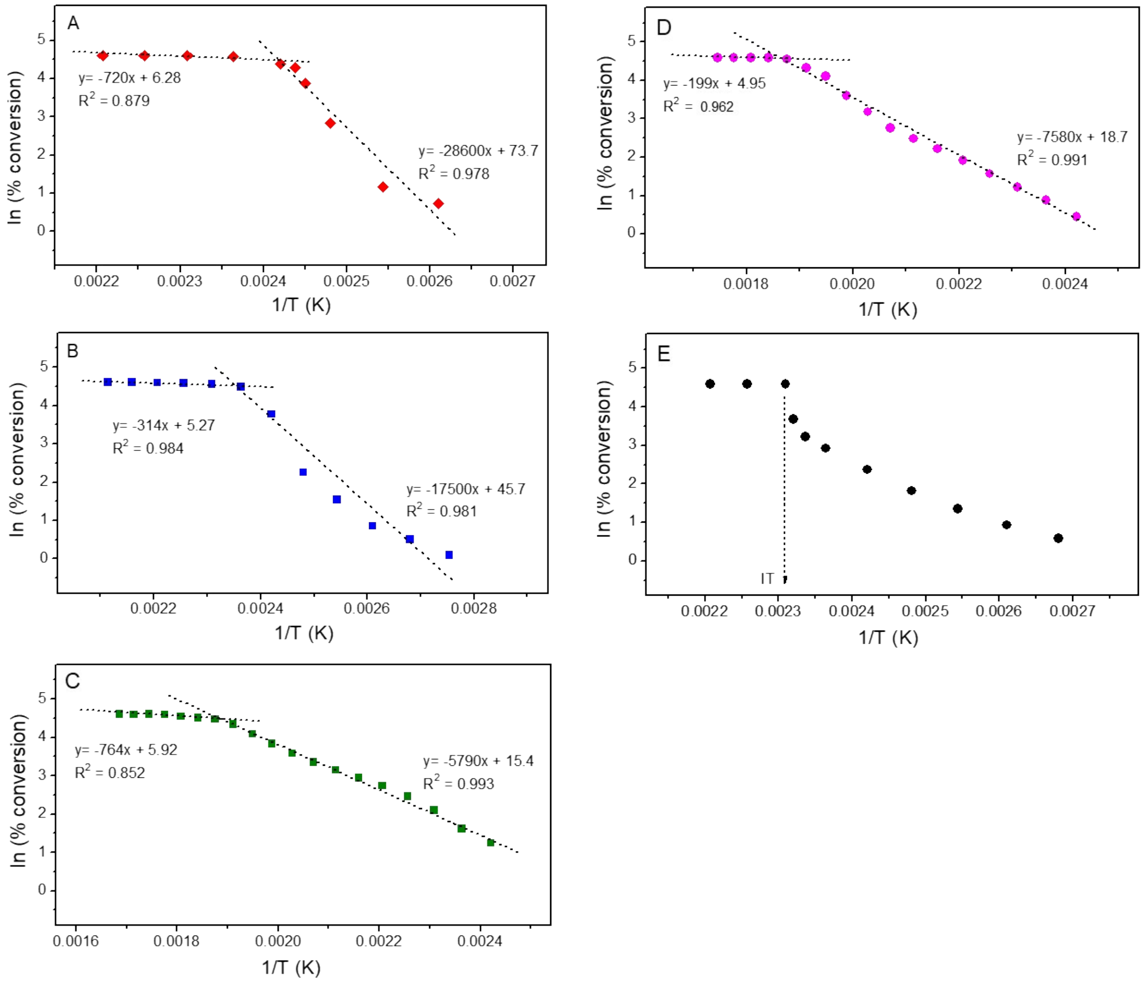

Fig. S6 Arrhenius plots for determining the ignition temperatures (ITs) of CO oxidation for (A) octahedral Pd@Rh/SBA15, (B) cubic Pd@Rh/SBA15 (C) cubic Rh/SBA15, and (D) Rh/C. The trend line analysis displays percentage conversion as a function of the reciprocal of temperature in Kelvin. (E) IT of CO oxidation for Pt/Al_2O_3 catalysts, which was supposed to be at 160 ^oC.

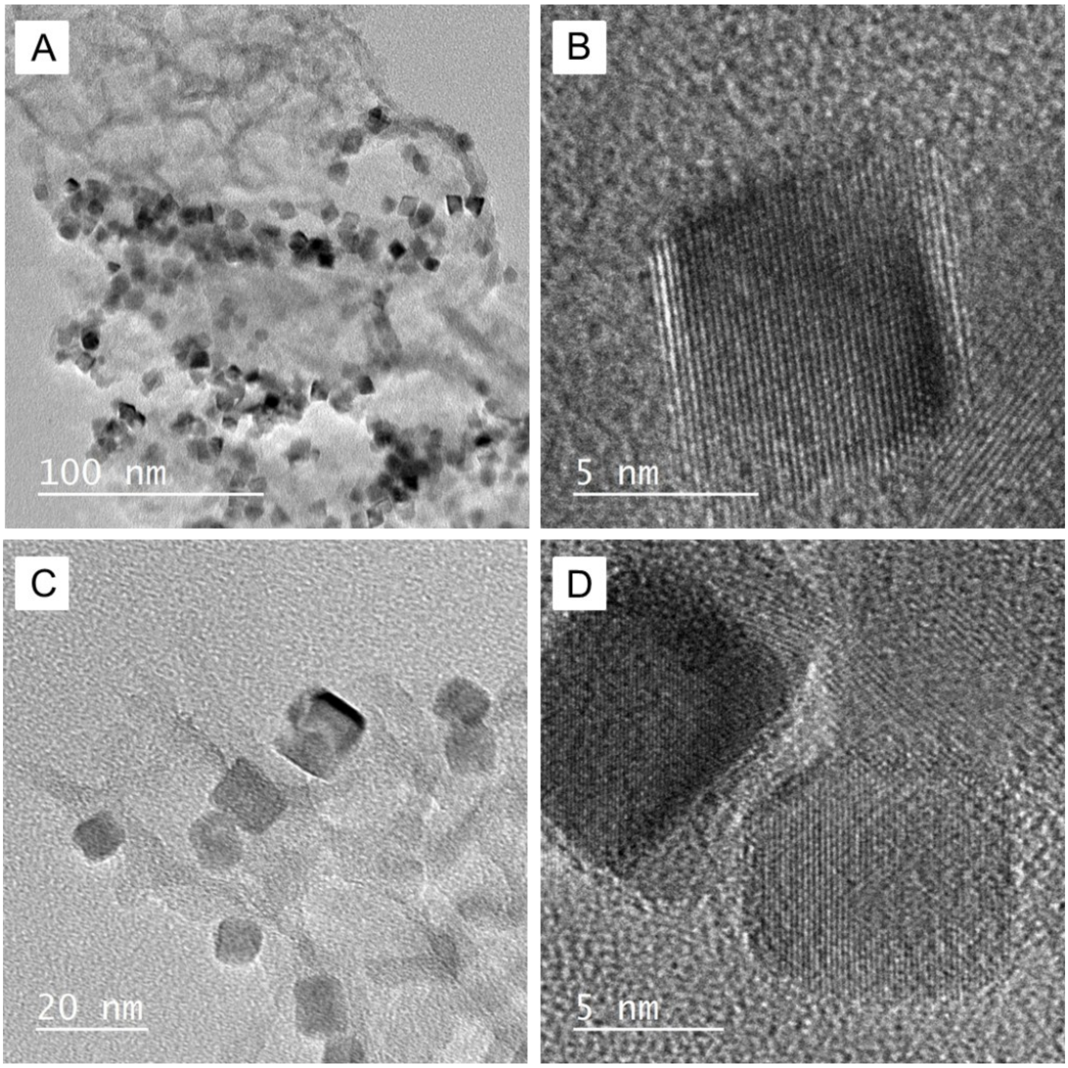

Fig. S7 TEM and high-resolution TEM images of (A, B) Pd@Rh/SBA15 octahedra and (C, D) Pd@Rh/SBA15 cubes after going through the catalytic CO oxidation reaction.